Celestial Mechanics and Dynamical Astronomy (2006) 94:155–171
DOI 10.1007/s10569-005-4626-3

SOLAR SAIL HALO ORBITS AT THE SUN–EARTH ARTIFICIAL L_1 POINT

HEXI BAOYIN[1] and COLIN R. MCINNES[2]
[1]*School of Aerospace, Tsinghua University, Beijing, 100084, China,*
e-mail: baoyin@tsinghua.edu.cn
[2]*University of Strathclyde, Glasgow, G1 1XJ, Scotland, UK,*
e-mail: colin.mcinnes@strath.ac.uk

(Received: 3 March 2005; revised: 15 August 2005; accepted: 31 October 2005)

Abstract. Halo orbits for solar sails at artificial Sun–Earth L_1 points are investigated by a third order approximate solution. Two families of halo orbits are explored as defined by the sail attitude. Case I: the sail normal is directed along the Sun-sail line. Case II: the sail normal is directed along the Sun–Earth line. In both cases the minimum amplitude of a halo orbit increases as the lightness number of the solar sail increases. The effect of the z-direction amplitude on x- or y-direction amplitude is also investigated and the results show that the effect is relatively small. In case I, the orbit period increases as the sail lightness number increases, while in case II, as the lightness number increases, the orbit period increases first and then decreases after the lightness number exceeds ~ 0.01.

Key words: halo orbit, libration point, solar sail

1. Introduction

During recent years, understanding of the classical collinear libration point halo orbits of the restricted three-body problem has undergone significant progresses (Farquhar, 1970, 1971; Farquhar and Kamel, 1973; Farquhar et al., 1977; Breakwell and Brown 1979; Farquhar et al., 1980; Richardson, 1980; Howell, 1984; Howell and Breakwell, 1984; Howell and Pernicka, 1988). Farquhar coined the name 'halo orbit' for a special family of periodic orbits around the libration points of restricted three-body problem and initiated the analytical study of halo orbits for an Earth–Moon libration point satellite (Farquhar, 1970, 1971; Farquhar et al., 1980). In addition, considering solar gravitational and lunar eccentricity perturbations, he analytically developed a quasi-periodic orbit around the Earth–Moon L_2 point (Farquhar and Kamel, 1973) and provided the frequency–amplitude relationship for large halo orbits. Based on the Lindstedt–Poincare method, Richardson (1980) developed a third order approximate solution for collinear libration point halo orbits of the circular restricted three-body problem and provided the minimum amplitude for a periodic orbit, along with the relationship between the amplitude and frequency correction. Breakwell and Brown (1979) developed a numerical method to find periodic orbits in the vicinity of libration points, and found some stable families of orbits. Extending the work of Breakwell et al. and Howell (Howell, 1984; Howell and Breakwell, 1984; Howell and Pernicka, 1988) investigated the libration point halo orbits of the restricted three-body problem for a wide range of mass ratio, and found many interesting stable periodic orbits such as the rectilinear halo orbit. In addition, by considering solar sails, McInnes et al. (McInnes and Simmons, 1992a, 1992b; McInnes 1993, 1999; McInnes et al., 1994) investigated a wide range of highly non-Keplerian orbits for solar sails, including heliocentric, geocentric and lunar libration point orbits. Most recently, Allan McInnes investigated solar sail halo orbits in circular restricted three-body systems (McInnes 2000). By considering the sail attitude as directed along the Sun-sail line, several types of on-axis and controlled off-axis halo orbits were investigated.

While the traditional restricted three-body problem possesses five fixed libration points, solar sails can generate an infinite number of artificial libration points inside certain allowed regions (McInnes et al., 1994; McInnes 1999). The objective of this paper is to investigate the properties of solar sail halo orbits around an artificial Sun–Earth L_1 point. Richardson formulated his analysis based on a Legendre Polynomial expansion of the Lagrangian, and defined a dimensionless distance based on the distance from the libration points to one of the primaries. In this paper, however, instead of Richardson's formulation we will adopt the formulation of Szebehely (1967) and McInnes (1999) with a Taylor series expansion of the potential function and solar pressure acceleration, and a dimensionless distance based on the Sun–Earth distance. According to McInnes (McInnes et al., 1994; McInnes 1999), one can find two ways to generate new artificial L_1 points: the sail normal vector directed along the Sun-sail line (case I) or along the Sun–Earth line (case II). Then by varying the sail lightness number (dimensionless ratio of solar radiation pressure force to solar gravitational force) from 0 to 1, new artificial L_1 points can be generated everywhere on x-axis from the classical L_1 point inwards to the Sun. In this paper we will investigate the orbit period of families of periodic halo orbits, the minimum amplitude for periodic orbits, and the effect of the out-of-plane amplitude and nonlinear frequency corrections for the two cases with third order approximate solutions.

2. Traditional Sun–Earth L_1 Halo Orbits

Neglecting the eccentricity of the Earth's orbit, the ideal Sun–Earth circular restricted three-body problem will be considered in this paper, with dimensionless equations of motion adopted (Szebehely, 1967). Let the Earth's mass be μ, and then Sun's mass be $1-\mu$. Then, including the lunar mass, for the Sun–Earth system $\mu = 3.04036 \times 10^{-6}$ (Richardson, 1980). In the coordinate system shown in Figure 1, the linearized equation of motion for the spacecraft around the L_1 point can be written as (Farquhar, 1977)

$$\ddot{x} - 2\dot{y} - (2B+1)x = 0 \tag{1a}$$

$$\ddot{y} + 2x + (B-1)y = 0 \tag{1b}$$

$$\ddot{z} + Bz = 0 \tag{1c}$$

where $B = 4.06107$ for Sun–Earth system. From the above equations, it is clear that the z-axis motion is independent of the others and is a simple harmonic oscillator with angular frequency $\sqrt{B}$. The xy-plane motion is coupled and it is easy to show that there are oscillatory and divergent modes and that the period of the oscillatory modes is different from that of the z-axis motion. Therefore, in the linear sense, the periodic motion is a set of Lissajous trajectories (Farquhar, 1977). However, it was shown that if nonlinear effects are considered, there are periodic halo orbits with the same in-plane and out-of-plane periods when the orbit amplitude is large enough (Farquhar, 1977, Farquhar et al., 1980; Richardson, 1980). It is found that in the Sun–Earth case, that type of halo orbit cannot exist unless the y-axis amplitude $A_y > 654,276\,\text{km}$ (Farquhar, 1977).

3. Solar Sail Sun–Earth L_1 Point Halo Orbits

While the location and period of classical halo orbits near the L_1 point are almost fixed, solar sails can provide new types of artificial Lagrange points

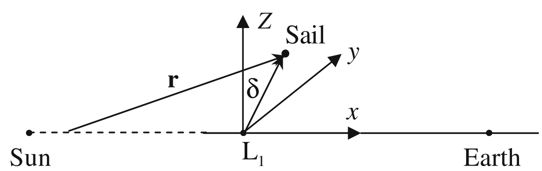

Figure 1. Coordinate system at the Sun–Earth libration point L_1.

(McInnes et al., 1994). In addition, by orientating the sail attitude appropriately, one can generate new families of L_1 point halo orbits related to the classical case. There are two methods of obtaining solar sail halo orbits at the L_1 point: one is to direct the sail normal vector orientated along the Sun-sail line (case I), and the other is to orient the sail normal along the Sun–Earth line (case II).

The equation of motion for a solar sail in the rotating frame can be written as (McInnes et al., 1994)

$$\ddot{\mathbf{r}} + 2\boldsymbol{\omega} \times \dot{\mathbf{r}} = \nabla V + \mathbf{a} \tag{2}$$

where $\boldsymbol{\omega}$ is the angular velocity vector of the rotating frame. In the dimensionless representation it is a unit vector along the z-axis and $\mathbf{r} = \left[r_x \; r_y \; r_z \right]^T$ is the position vector of the sail with respect to the centre-of-mass of the Sun–Earth system. A group of dimensionless variables are again adopted (Szebehely, 1967). The effective potential function V is defined as

$$V = \left(\frac{1-\mu}{r_1} + \frac{\mu}{r_2} \right) + \frac{1}{2} (\boldsymbol{\omega} \times \mathbf{r}) \cdot (\boldsymbol{\omega} \times \mathbf{r}) \tag{3}$$

while the solar radiation pressure acceleration $\mathbf{a}$ is defined as

$$\mathbf{a} = \beta \frac{1-\mu}{r_1^2} \frac{(\mathbf{r}_1 \cdot \mathbf{n})^2}{r_1^2} \mathbf{n} \tag{4}$$

where $\mathbf{n}$ is sail unit normal vector and β is the sail lightness number related to the sail areal density σ by $\beta = 1.53/\sigma \left[g \; m^{-2} \right]$ (McInnes et al., 1994). Then in Equation (2), setting

$$\ddot{\mathbf{r}} = \dot{\mathbf{r}} = 0 \tag{5}$$

$$r_y = 0, \; r_z = 0 \tag{6}$$

one can find a continuum of new artificial collinear points along the Sun–Earth line parameterized by the sail lightness number. In this paper we only focus on the L_1 point, since the case of the L_2 and L_3 points can be studied in a similar manner. As noted, the location of the artificial L_1 point is a function of the lightness number. Figure 2 shows the relationship between the sail lightness number and location of the L_1 point.

To investigate halo orbits near the artificial L_1 point, we will approximate the equations of motion in the neighborhood of that point. Below we solve the third order solution of this approximated equation following the methodology of Richardson (1980), but adopting the three-body system formulation from Szebehely (1967), and expanding the potential function

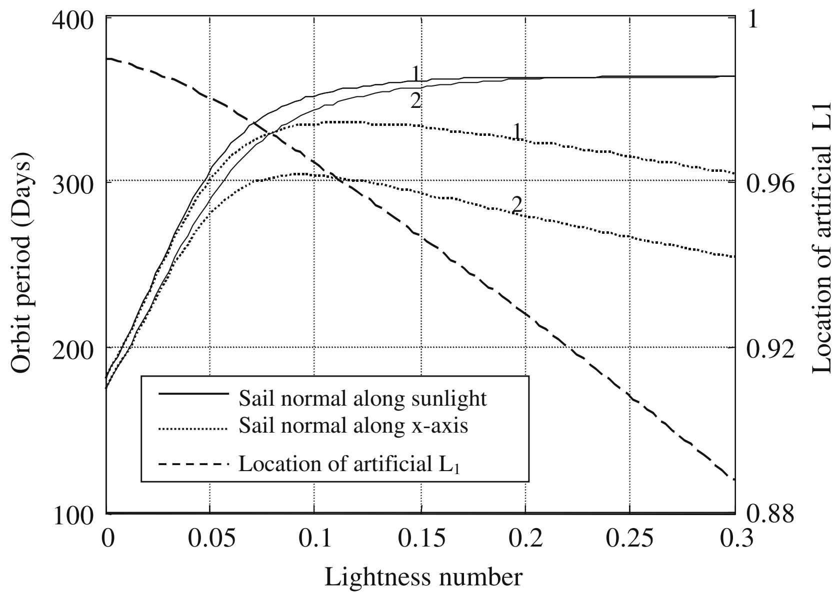

Figure 2. Orbit period and location of the artificial L_1 point (1): out-of-plane period; (2): in-plane period.

and solar radiation pressure acceleration around the artificial L_1 points with Taylor series. Then, the third order approximation of the equations of motion can be represented as

$$\ddot{\boldsymbol{\delta}} + 2\boldsymbol{\omega} \times \dot{\boldsymbol{\delta}} = F_r|_{L1}\,\boldsymbol{\delta} + F_{rr}|_{L1}\,\boldsymbol{\delta}^2 + F_{rrr}|_{L1}\,\boldsymbol{\delta}^3 + o(\boldsymbol{\delta}^4) \tag{7}$$

where $\boldsymbol{\delta} = \begin{bmatrix} x & y & z \end{bmatrix}^T$, and F_r, F_{rr}, F_{rrr} are the first, second and third derivative matrices of the Taylor expansion of $\nabla V + \mathbf{a}$, respectively. We note that mixed terms are included in the higher order terms, for example the xy product is included in the $\boldsymbol{\delta}^2$ term. Then, if this equation is represented in scalar form it yields

$$\begin{aligned} \ddot{x} - 2\dot{y} - (2B + 1 - A)x = {} & 3C(2x^2 - y^2 - z^2) + 4Dx(2x^2 - 3y^2 - 3z^2) \\ & \times 2E(3x^2 - 2y^2 - 2z^2) + 8Fx(x^2 - 2y^2 - 2z^2) \end{aligned} \tag{8a}$$

$$\ddot{y} + 2\dot{x} + (B - 1)y = -6Cxy - 3Dy(4x^2 - y^2 - z^2) \tag{8b}$$

$$\ddot{z} + Bz = -6Cxz - 3Dz(4x^2 - y^2 - z^2) \tag{8c}$$

where in case I, $A = E = F = 0$, and B, C, D are explicit functions of the location of L_1 and so the sail lightness number. In case II, A, E, F arise from **a** and are explicit functions of the location of L_1 and so the sail lightness number; while B, C, D arise from $\nabla V$and are explicit functions of the location of L_1 only (See Equations (A1)).

4. Third Order Solution

To use the Lindstedt–Poincare method to obtain the third order-approximate solution, we introduce a new parameter

$$\tau = \varepsilon t \tag{9}$$

and define the primes to represent the derivative with respect to this new parameter, τ. Then, Equations (8) are transformed to Equations (A2).

To solve the third order solution, we assume the solutions are of form

$$\varepsilon = 1 + \varepsilon_1 + \varepsilon_2 \tag{10a}$$

$$x = x_1 + x_2 + x_3 \tag{10b}$$

$$y = y_1 + y_2 + y_3 \tag{10c}$$

$$z = z_1 + z_2 + z_3 \tag{10d}$$

and here assume that ε_1 and ε_2 are of first and second order respectively, while the out-of-plane period correction $\Delta = (\lambda^2 - B)$ is of second order. Then, substituting Equations (10) into Equations (A2), and grouping the same order terms, the first, second and third order groups of equations can be obtained as shown in Equations (A3) through (A5). To solve these three groups of equations, first order generating solutions are assumed as

$$x_1 = X \cos \lambda\tau \tag{11a}$$

$$y_1 = kX \sin \lambda\tau \tag{11b}$$

$$z_1 = \eta X \cos \lambda\tau \tag{11c}$$

where, $\eta = Z/X$ is an independent parameter, defined as the ratio of z- and x-axis amplitude and

$$Y/X = k = -\frac{\lambda^2 + \left.\frac{\partial(V_x + a^x)}{\partial x}\right|_{L1}}{2\lambda} \tag{12}$$

is the ratio of the y- and x-axis amplitudes, where $\mathbf{a} = \left[a^x \; a^y \; a^z \right]^T$, and $\pm i\lambda$ is the imaginary solution of characteristic equation

$$\lambda^4 + (2 + A - B)\lambda^2 + (1 - A + B + AB - 2B^2) = 0 \tag{13}$$

Substituting the first order solutions into the second order equations, and then from the first two Equations (A4a) and (A4b), it is clear that $\varepsilon_1 = 0$, otherwise the second order solution will include secular terms. Canceling the secular terms, the second order solutions can be obtained as

$$x_2 = P_{20} + P_2 \cos 2\lambda\tau \tag{14a}$$

$$y_2 = Q_2 \sin 2\lambda\tau \tag{14b}$$

$$z_2 = M_2 [\cos 2\lambda\tau - 3] \tag{14c}$$

where the coefficients are listed in Equations (A8). Finally, substituting the first and second order solutions into the third order equations, the third group of equations are obtained as shown in Equations (A9). By canceling the secular terms in the x- and y-directions, we can obtain the frequency adjustment ε_2 and amplitude relation as

$$2\lambda q_{31} + (B - 1 - \lambda^2) p_{31} = 0 \tag{15}$$

where p_{31} and q_{31} are defined in (A10). In this equation we can further represent ε_2 by the amplitudes of the y-direction (or x-direction) and z-direction, and substituting ε_2 into m_{31} so that the relationship between the frequency correction and amplitudes can be obtained as

$$\Delta = qY^2 + mZ^2 \tag{16}$$

where the coefficients p and m are very lengthy expressions which can be obtained from other coefficients listed in the Appendix. Setting $Z = 0$ in this equation one can obtain the minimum value of the amplitude for a periodic orbit as

$$Y^2 \geqslant \Delta / p \tag{17}$$

Then, after canceling the secular terms, the third order solutions can be obtained as

$$x_3 = P_3 \cos 3\lambda\tau \tag{18a}$$

$$y_3 = Q_3 \sin 3\lambda\tau \tag{18b}$$

$$z_3 = M_3 \cos 3\lambda\tau \tag{18c}$$

where the coefficients are listed in Equation (A11).

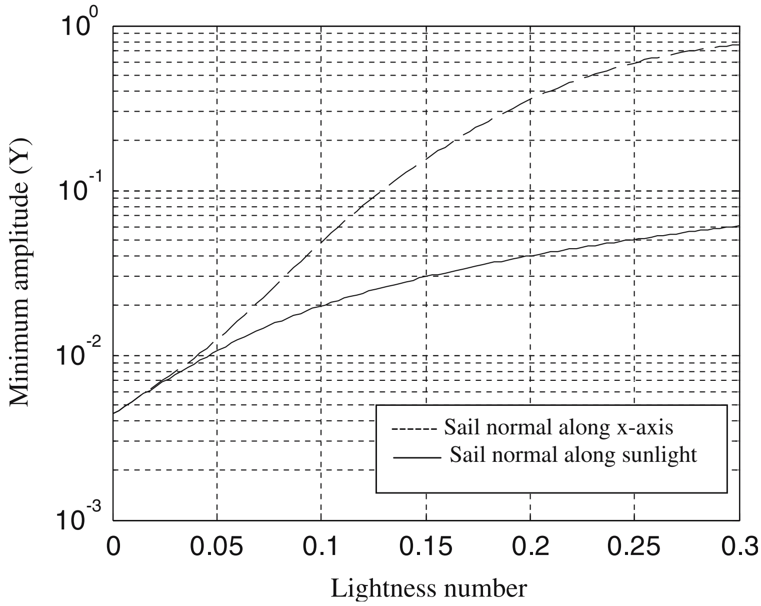

Figure 3. y-direction minimum amplitude Y.

5. Results and Discussion

Setting $\beta = 0$ in the above equations, only one L_1 point, the classical point, can be obtained and all results degenerate to the case of Richardson's results (Richardson, 1980). For $\beta \neq 0$, Figure 2 illustrates the variation of the location of artificial L_1 point and the in-plane and out-of-plane period of the linearized systems for both case I and II. It can be seen that the in-plane and out-of-plane orbit periods of case I approaches the period of the Earth's orbit (1 year) as the lightness number increases, and in case II, the in-plane and out-of-plane periods are somewhat different, and have a turning point as the lightness number increases.

Figure 3 illustrates the relationship between the minimum amplitude and the sail lightness number. In both cases the minimum amplitude will increase as the lightness number increases, but the increment is faster in case II than case I. The amplitude reaches 0.02 (of order 3,000,000 km in dimensional units) when $\beta = 0.1$ in case I and 0.05 in case II. Note that from the expansion of the higher order terms of the potential function and solar pressure acceleration, it can be shown that the coefficients of the fourth order terms are two orders larger than the third order terms, so the validity of the range of the approximation is $\|\delta\| < 0.01$ (about 1,500,000 km in the dimensional units).

Figures 4 and 6 illustrate the variation of the y-direction amplitude with lightness number, with the z-direction amplitude set as 0, 0.002, 0.004 and 0.006 (in dimensional units, of order 0, 300,000, 600,000 and 900,000 km respectively). The figures show that the effect of z-direction amplitude on y-direction amplitude is relatively small in both cases.

Figures 5 and 7 show some halo orbits around the artificial L_1 point. Here we fix the lightness number at $\beta = 0.02$, and set the z-direction amplitude as 0.001, 0.002 and 0.003. Note that only the counterclockwise orbits are shown here, but setting a negative value for η one can obtain clockwise orbits.

Figures 8 and 9 show the relation between lightness number and ε_2 and λ. Comparing with the orbit period, the second order frequency adjustments ε_2 are very small in both cases. It is found that λ approaches 1 in case I, while λ decreases and then increases in case II as the lightness number increases. The frequency correction of case I is smaller than that of the case II. This shows that in practice it is easier to achieve larger orbits in case I.

6. Conclusions

Artificial Sun–Earth L_1 point halo orbits are investigated by using a third order-approximate solution. The sail attitude is considered with the sail normal directed along the Sun-sail line (case I) and along the Sun–Earth

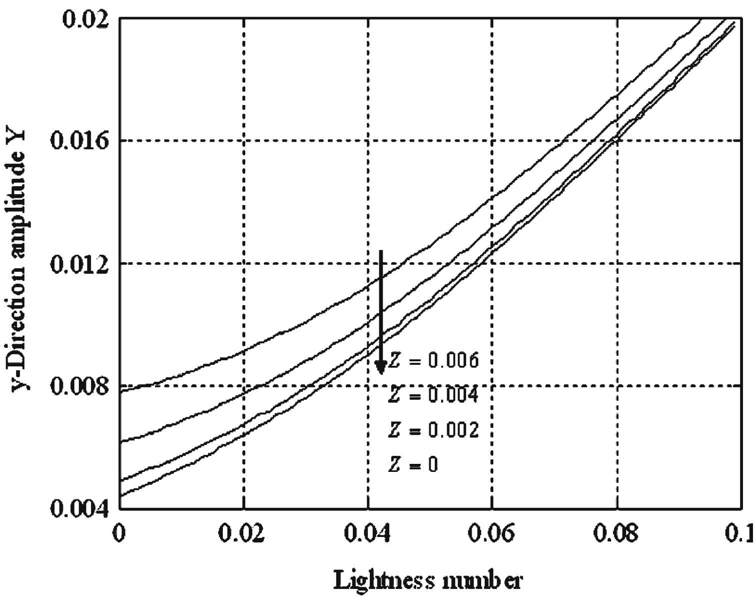

Figure 4. Y with various Z (case I).

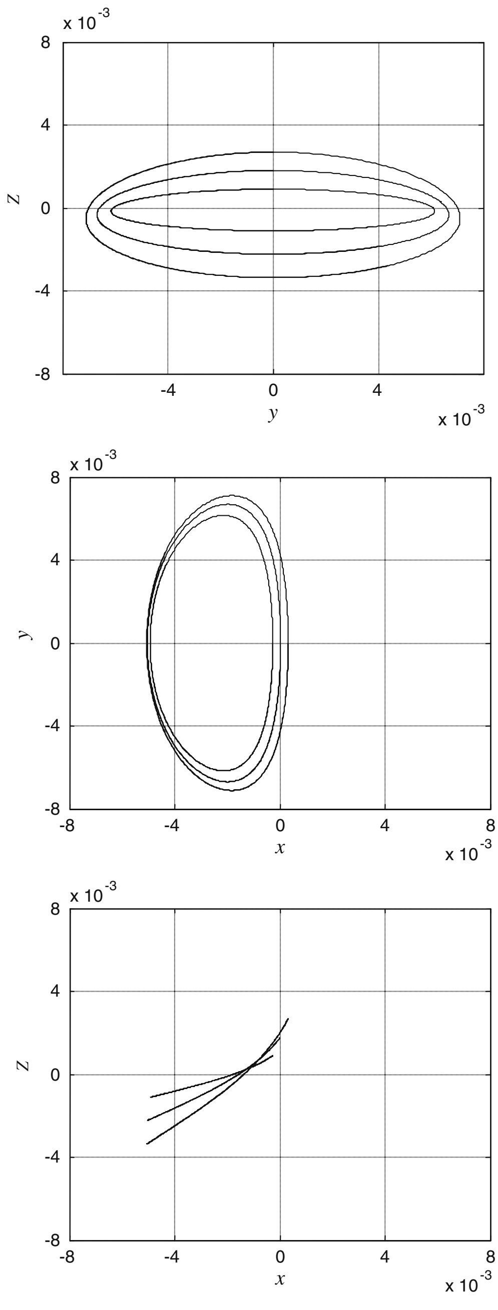

Figure 5. Halo orbits around the artificial L_1 point (case I, $\beta = 0.02$, $Z = 0.001$, 0.002, 0.003).

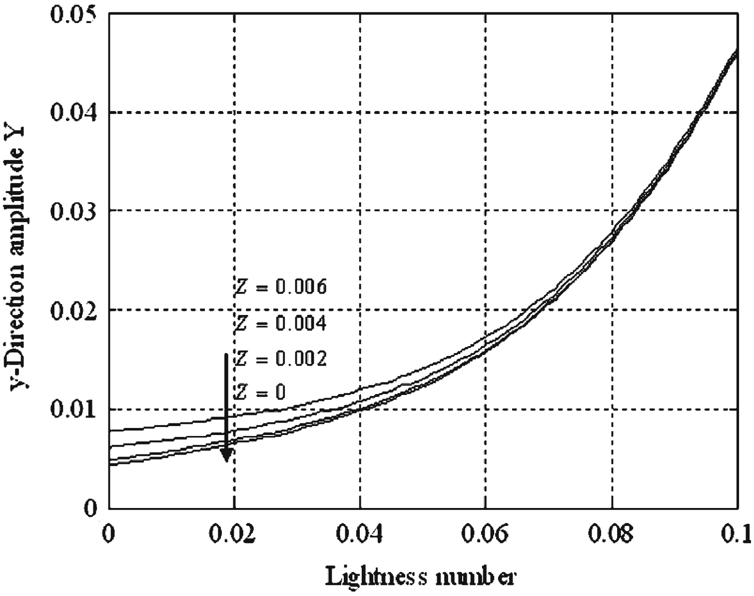

Figure 6. Y with various Z (case II).

line (case II). In both cases the minimum amplitude of a halo orbit increases as the lightness number increases, while in case II the increase is faster than case I. The effect of z-direction amplitude on y-direction amplitude is relatively small. In both cases the second order frequency adjustments are small. Because of the rapid increase in minimum amplitude for such periodic orbits, the range of location available for periodic orbits is limited, but one can, in principle, design a solar sail halo orbit at any point between the Sun and the L_1 point.

Appendix

In the case I, $\mathbf{a} = [a^x, a^y, a^z]^T$,

$$B = -\frac{\left(V_{xx} + a_z^x\right)\big|_{L1}}{2} \tag{A1a}$$

$$C = \frac{\left(V_{xxx} + a_{xx}^x\right)\big|_{L1}}{12} \tag{A1b}$$

$$D = \frac{\left(V_{xxxx} + a_{xxx}^x\right)\big|_{L1}}{48} \tag{A1c}$$

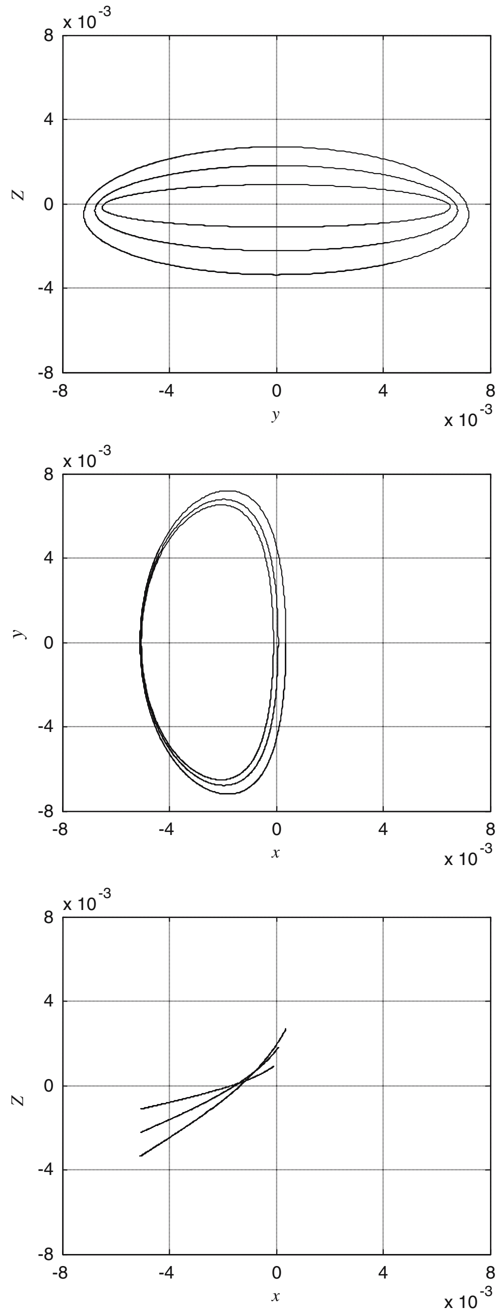

Figure 7. Halo orbits around the artificial L_1 point (case II, $\beta = 0.02$, $Z = 0.001$, 0.002, 0.003).

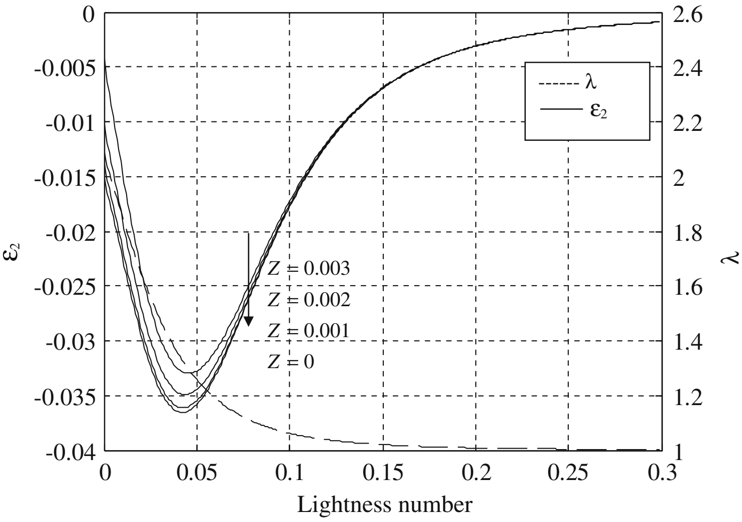

Figure 8. Zero- and 2nd-order frequencies with various Z (case I).

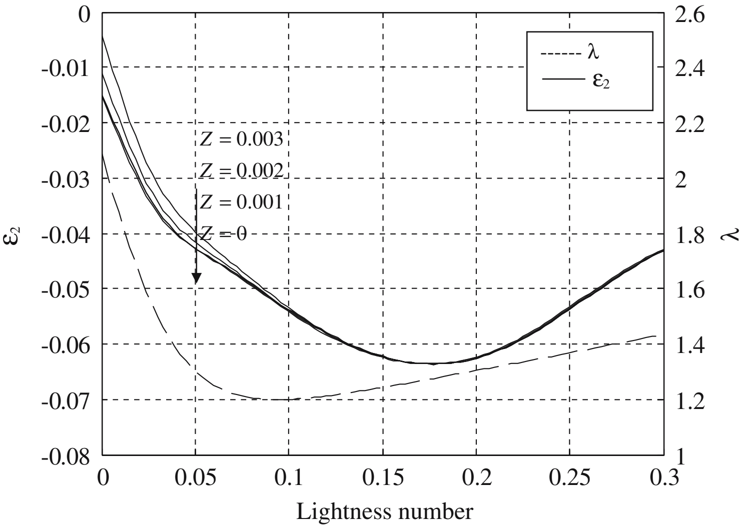

Figure 9. Zero- and 2nd-order frequencies with various Z (case II).

In the case II, $\mathbf{a} = [a, 0, 0]^T$,

$$B = -V_{zz}|_{L1} \tag{A1d}$$

$$C = \frac{V_{xxx}|_{L1}}{12} \tag{A1e}$$

$$D = \frac{V_{xxxx}|_{L1}}{48} \tag{A1f}$$

$$A = -\, a_x|_{L1} \tag{A1g}$$

$$E = \frac{a_{xx}|_{L1}}{12} \tag{A1h}$$

$$F = \frac{a_{xxx}|_{L1}}{48} \tag{A1i}$$

$$\begin{aligned} &\varepsilon^2 x'' - 2\varepsilon y' - (2B + 1 - A)x \\ &\quad = 3C(2x^2 - y^2 - z^2) + 4Dx(2x^2 - 3y^2 - 3z^2) \\ &\qquad + 2E(3x^2 - 2y^2 - 2z^2) + 8Fx(x^2 - 2y^2 - 2z^2) \end{aligned} \tag{A2a}$$

$$\varepsilon^2 y'' + 2\varepsilon x' + (B - 1)y = -6Cxy - 3Dy(4x^2 - y^2 - z^2) \tag{A2b}$$

$$\varepsilon^2 z'' + \lambda^2 z = -6Cxz - 3Dz(4x^2 - y^2 - z^2) + (\lambda^2 - B)z \tag{A2c}$$

First order equations

$$x_1'' - 2y_1'' - (2B + 1 - A)x_1 = 0 \tag{A3a}$$

$$y_1'' + 2x_1' + (B - 1)y_1 = 0 \tag{A3b}$$

$$z_1'' + \lambda^2 z_1 = 0 \tag{A3c}$$

Second order equations

$$\begin{aligned} x_2'' - 2y_2' - (2B + 1 - A)x_2 = &-2\varepsilon_1 x_1'' + 2\varepsilon_1 y_1' \\ &+ (6C + 6E)x_1^2 - (3C + 4E)(y_1^2 + z_1^2) \end{aligned} \tag{A4a}$$

$$y_2'' + 2x_2' + (B - 1)y_2 = -2\varepsilon_1 y_1'' - 2\varepsilon_1 x_1' - 6Cx_1 y_1 \tag{A4b}$$

$$z_2'' + \lambda z_2 = -2\varepsilon_1 z_1'' - 6Cx_1 z_1 \tag{A4c}$$

Third order equations

$$\begin{aligned} &x_3'' - 2y_3' - (2B + 1 - A)x_3 \\ &\quad = -\varepsilon_1^2 x_1'' - 2\varepsilon_2 x_1'' - 2\varepsilon_1 x_2'' + 2\varepsilon_2 y_1' + 2\varepsilon_1 y_2' \\ &\qquad + (12C + 12E)x_1 x_2 - (6C + 8E)(y_1 y_2 + z_1 z_2) \\ &\qquad + (8D + 8F)x_1^3 - (12D + 16F)(x_1 y_1^2 + x_1 z_1^2) \end{aligned} \tag{A5a}$$

$$y_3'' + 2x_3'' + (B-1)y_3 = -\varepsilon_1^2 y_1'' - 2\varepsilon_2 y_1'' - 2\varepsilon_1 y_2'' - 2\varepsilon_2 x_1' + 2\varepsilon_1 x_2' \\ -6C(x_1 y_2 + x_2 y_1) - 3Dy_1(4x_1^2 - y_1^2 - z_1^2) \quad \text{(A5b)}$$

$$z_3'' + \lambda^2 z_3 = -\varepsilon_1^2 z_1'' - 2\varepsilon_2 z_1'' - 2\varepsilon_1 z_2'' + (\lambda^2 - B)z_1 \\ -6C(x_1 z_2 + x_2 z_1) - 3Dz_1(4x_1^2 - y_1^2 - z_1^2) \quad \text{(A5c)}$$

After substituting the first order solution into second order equations

$$x_2'' - 2y_2' - (2B + 1 - A)x_2 = p_{20} + p_2 \cos 2\lambda\tau \quad \text{(A6a)}$$

$$y_2'' + 2x_2' + (B-1)y_2 = q_2 \sin 2\lambda\tau \quad \text{(A6b)}$$

$$z_2'' + \lambda z_2 = m_2 \cos 2\lambda\tau \quad \text{(A6c)}$$

where

$$p_{20} = \frac{X^2}{2}\left[(6C + 6E) - (3C + 3E)(k^2 + \eta^2)\right] \quad \text{(A7a)}$$

$$p_2 = \frac{X^2}{2}\left[(6C + 6E) + (3C + 3E)(k^2 - \eta^2)\right] \quad \text{(A7b)}$$

$$q_2 = -3CkX^2 \quad \text{(A7c)}$$

$$m_2 = -3C\eta X^2 \quad \text{(A7d)}$$

Coefficients of the second order solutions

$$R_2 = B - 2B^2 + 4B\lambda^2 + (1 - 4\lambda^2)^2 + A(B - 1 - 4\lambda^2) \quad \text{(A8a)}$$

$$P_2 = \frac{4\lambda q_2 + (B - 1 - 4\lambda^2)p_2}{R_2} \quad \text{(A8b)}$$

$$Q_2 = \frac{4\lambda p_2 + (A - 1 - 2B - 4\lambda^2)q_2}{R_2} \quad \text{(A8c)}$$

$$P_{20} = \frac{p_{20}}{A - 2B - 1} \quad \text{(A8d)}$$

$$M_2 = \frac{\eta C X^2}{\lambda^2} \quad \text{(A8e)}$$

After substituting the first and second order solutions into the third order equations

$$x_3'' - 2y_3' - (2B + 1 - A)x_3 = p_{31}\cos\lambda\tau + p_{33}\cos 3\lambda\tau \quad \text{(A9a)}$$

$$y_3'' + 2x_3' + (B - 1)y_3 = q_{31}\sin\lambda\tau + q_{33}\sin 3\lambda\tau \quad \text{(A9b)}$$

$$z_3'' + \lambda^2 z_3 = m_{31}\cos\lambda\tau + m_{33}\cos 3\lambda\tau \quad \text{(A9c)}$$

where

$$p_{31} = \left\{ \frac{2\varepsilon_2(\lambda^2 + k\lambda)}{X^2} + \frac{(6C + 6E)(2P_{20} + P_2)}{X^2} - (6C + 8E)\left(\frac{1}{2X^2}kQ_2 - \frac{5C\eta^2}{2\lambda^2}\right) + (6D + 6F) - (3D + 2F)\left(k^2 + 3\eta^2\right) \right\} X^3 \quad \text{(A10a)}$$

$$p_{33} = \left\{ \frac{(6C + 6E)P_2}{X^2} - (6C + 8E)\left(-\frac{1}{2X^2}kQ_2 + \frac{C\eta}{2\lambda^2}\right) + (2D + 2F) - (3D + 2F)\left(\eta^2 - k^2\right) \right\} X^3 \quad \text{(A10b)}$$

$$q_{31} = \left\{ \frac{2\varepsilon_2(k\lambda^2 + \lambda)}{X^2} - 6C\left[\frac{Q_2 + k(2P_{20} - P_2)}{2X^2}\right] - 3Dk\left[1 - \frac{3}{4}k^2 - \frac{1}{4}\eta^2\right] \right\} X^3 \quad \text{(A10c)}$$

$$q_{33} = \left\{ -6C\left[\frac{kP_2 + Q_2}{2X^2}\right] - 3D\left[k + \frac{1}{4}k^3 - \frac{1}{4}k\eta^2\right] \right\} X^3 \quad \text{(A10d)}$$

$$m_{31} = \left\{ \frac{(2\varepsilon_2\lambda^2 + \Delta)}{X^2} - 6C\left[\frac{(2P_{20} + P_2)}{2X^2} - \frac{5C}{2\lambda^2}\right] - 3D\left(3 - \frac{k^2}{4} - \frac{3\eta^2}{4}\right) \right\} \eta X^3 \quad \text{(A10e)}$$

$$m_{33} = \left\{ -6C\left(\frac{C\eta}{2\lambda^2} + \frac{\eta P_2}{2X^2}\right) - 3D\left(\eta + \frac{k^2\eta}{4} - \frac{\eta^3}{4}\right) \right\} X^3 \quad \text{(A10f)}$$

Coefficients of the third order solutions

$$R_3 = B - 2B^2 + 9B\lambda^2 + (1 - 9\lambda^2)^2 + A(B - 1 - 9\lambda^2) \quad \text{(A11a)}$$

$$P_3 = \frac{6\lambda q_{33} + (B - 1 - 9\lambda^2) p_{33}}{R_3} \tag{A11b}$$

$$Q_3 = \frac{6\lambda p_{33} + (A - 2B - 1 - 9\lambda^2) q_{33}}{R_3} \tag{A11c}$$

$$M_3 = -\frac{m_{33}}{8\lambda^2} \tag{A11d}$$

References

Breakwell, J. V. and Brown, J. V.: 1979, 'The 'Halo' family of 3-dimensional periodic orbits in the earth–moon restricted 3-body problem', *Celest. Mech.* **20**, 389–404.

Farquhar, R. W.: 1970, *The Control and Use of Libration-Point Satellite*, NASA TR R-346, Goddard Space Flight Center, Greenbelt, MD.

Farquhar, R. W.: 1971, *The Utilization of Halo Orbits in Advanced Lunar Operations*, NASA TN D-6365, Goddard Space Flight Center, Greenbelt, MD.

Farquhar, R. W. and Kamel, A. A.: 1973, 'Quasi-periodic orbits about the thanslunar libration point', *Celest. Mech.* **7**, 458–473.

Farquhar, R. W., Muhonen, D. P. and Richardson, D. L.: 1977, 'Mission design for a halo orbiter of the earth', *J. Spacecraft Rockets* **14**(3), 170–177.

Farquhar, R. W., Muhonen, D. P., Newman, C. R. and Heuberber, H. S.: 1980, 'Trajectories and orbital maneuvers for the first libration-point satellite', *J. Guidance Control* **3**, 549–554.

Howell, K. C.: 1984, 'Three-dimensional, periodic, 'halo' orbit', *Celest. Mech.* **32**, 53–71.

Howell, K. C. and Breakwell, J. V.: 1984, 'Almost rectilinear halo orbit', *Celest. Mech.* **32**, 29–52.

Howell, K. C. and Pernicka, H. J.: 1988, 'Numerical determination of lissajous trajectories in the restricted three-body problem', *Celest. Mech.* **41**, 107–124.

McInnes, A. I. S.: 2000, *Strategies for Solar Sail Mission Design in the Circular Restricted Three-Body Problem*, M.S. Thesis, Purdue University, West Lafayette.

McInnes, C. R. and Simmons, J. F. L.: 1992a, 'Solar Sail Halo orbit I: Heliocentric Case', *J. Spacecraft Rockets* **29**(4), 466–471.

McInnes, C. R. and Simmons, J. F. L.: 1992b, 'Solar Sail Halo orbit I: Geocentric Case'. *J. Spacecraft Rockets* **29**(4), 472–479.

McInnes, C. R.: 1993, 'Solar sail trajectories at the lunar L$_2$ lagrange point', *J. Spacecraft Rockets* **30**(6), 782–784.

McInnes, C. R., Mcdonald, A. J. C., Simmons, J. F. L. and MacDonald, E. W.: 1994, 'Solar sail parking in restricted three-body system', *J. Guidance, Control, Dynamics* **17**(2), 399–406.

McInnes, C. R.: 1999, *Solar Sailing: Technology, Dynamics and Mission Applications*, Springer-Verlag, London.

Richardson, D. L.: 1980, 'Analytic construction of periodic orbits about the collinear points', *Celest. Mech.* **22**, 241–253.

Szebehely, V.: 1967, *Theory of Orbits: The Restricted Problem of Three Bodies*. Academic Press, New York.